JOURNAL OF Applied Polymer SCIENCE

Development of Active Barrier Systems for Poly(ethylene terephthalate)

Kamal Mahajan, Elizabeth A. Lofgren, Saleh A. Jabarin
Chemical and Environmental Engineering, Polymer Institute, The University of Toledo, Toledo, Ohio 43606-3390
Correspondence to: S. A. Jabarin (E-mail: saleh.jabarin@utoledo.edu)

ABSTRACT: Copolymers of Poly(ethylene terephthalate) (PET) were synthesized by the melt polymerization of terephthalic acid (TPA) with ethylene glycol (EG) and with each of the active oxygen scavengers; monoolein (MO) and 3-cyclohexene-1,1-dimethanol (CHEDM) in separate compositions. Proton nuclear magnetic resonance spectroscopy (^{1}H NMR) and 2D correlation spectroscopy (COSY) indicated that PET had reacted with both MO and CHEDM at their hydroxyl end groups. Oxygen barrier properties of the MO and CHEDM copolymers exhibited improvements of up to 40%, in comparison to an unmodified commercial PET. Effects of the oxygen scavengers on the copolymers' physical properties were investigated in terms of their crystallization, melting, and rheological behaviors. Both types of copolymers showed decreases in peak melting temperatures with increased scavenger concentrations and also crystallized more slowly as the scavenger concentrations increased. The PET/MO copolymer showed non-Newtonian rheological behavior with higher MO concentration; while the PET/CHEDM copolymers showed Newtonian behavior within the studied range of CHEDM concentrations. © 2013 Wiley Periodicals, Inc. J. Appl. Polym. Sci. 129: 2196–2207, 2013

KEYWORDS: copolymers; polyesters; rheology; thermal properties

Received 11 September 2012; accepted 16 December 2012; published online 15 January 2013
DOI: 10.1002/app.38930

INTRODUCTION

Poly(ethylene terephthalate) (PET) is a widely used polymer in the food and beverage packaging industry. PET exhibits many attractive properties such as excellent clarity, good gas and flavor component barrier, ease of melt processing, and acceptable thermal resistance and mechanical strength. The oxygen barrier properties of PET are acceptable for many food and beverage products. Improvements are, however, needed in order to meet the requirements for packaging highly oxygen sensitive food and beverage products. Various methods have been used to reduce the inherent oxygen permeability of PET as a passive (nonreactive) polymer. These include structure and morphology manipulation,[1–4] copolymerization[5–9], and the use of nanocomposites.[10–21] Such strategies have provided limited levels of barrier property improvement. In the case of nanocomposites, the formation of haze and nanoparticle agglomeration as well as phase separation between the nanoparticles and the PET matrix continue to be very challenging problems.[14,15]

The addition of an active oxygen scavenger directly into the PET polymer can significantly improve the oxygen barrier properties of PET films and containers. The PET active barrier system can be achieved by blending through extrusion and reactive extrusion or by direct polymerization of PET monomer with the incorporation of the scavenging moiety as a copolymer.

An active oxygen scavenger is a substance capable of intercepting and scavenging oxygen by undergoing a chemical reaction with the oxygen as it permeates through the polyester packaging wall. Amosorb® and Oxbar® systems[22,23] are examples where oxidizable groups were introduced into the main chain of the polymer matrix. The Amosorb® technology[22] consists of the preparation of copolyesters incorporating polybutadiene (PBD) segments into the main chain of PET. The PBD segments confer significant oxygen-absorbing capacity at loadings of 4–12 wt %. The PBD segments are long and mobile enough to be able to aggregate into somewhat organized olefin-rich domains with diameters of approximately 0.5–1 μm that can substantially affect the optical properties of the solid copolyester. The Oxbar® system[23] consists of an extruded blend of the aromatic polyamide MXD6 and PET, along with a metal (oxidation) catalyst. The reaction with oxygen causes chain scission, which ultimately results in low molecular weight products from the amide sites, which are attacked along the chain. Blends of MXD6 and PET may not show good clarity, since they are incompatible and hence produce a multiphase blend.

No published reports have been found describing attempts to prepare side-chain modified PET in which pendant groups can be readily (or controllably) oxidized. The current research has, therefore, focused on the use of pendant C=C double bonds designed to minimize rupture of the polymer backbone during oxidation. For this purpose, substituted aliphatic unsaturated compounds and substituted cyclic olefinic compounds were used as oxygen scavengers and incorporated into PET to improve its active barrier properties.

The oxygen scavengers used in this research are monoolein (MO), which is a branched diol with mono-unsaturation in its side chain and 3-cyclohexene-1,1-dimethanol (CHEDM), which is a branched diol with cycloalkene unsaturation in its side chain. The oxidizable moieties are cyclohexene side groups, and unsaturated side groups bound to the backbone. An important advantage of both scavengers is that the unsaturated groups are present as side chains to the main long PET chains. Any oxidative cleavage will therefore occur at the double bond (which is not a part of the main PET chain) and will not results in any significant molecular weight loss. Another advantage of selecting a cyclic olefinic group is that it does not fragment as it oxidizes, thus avoiding the problem of imparting oxidation byproducts to packaged materials.[24,25]

In this article, we discuss synthesis of the PET/scavenger copolymers and effects of the oxygen scavengers on oxygen barrier, rheological, and thermal properties of PET. In a second article, we also discuss the effects of the oxygen scavengers on the oxygen barrier properties of PET as well as determination of oxidation by-products of the copolymer samples and a methodology for determining the effectiveness (or scavenging capacity) of the oxygen scavengers.

EXPERIMENTAL

Materials

Terephthalic acid (TPA) was donated by Amoco Chemical Company, Rosemont, IL. Ethylene glycol (EG) (polyester grade) was purchased from Superior Solvents and Chemicals, Cincinnati, OH. MO was obtained from City Chemical, West Haven, CT. The CHEDM, cobalt acetate, tetramethylammonium hydroxide, phosphoric acid, and antimony trioxide materials were obtained from Acros Organics, Pittsburgh, PA. Chloroform and trifluoroacetic acid (d-TFA) were purchased from Fisher Scientific, Fair Lawn, NJ. Chloroform (deuterated) was purchased from Cambridge Isotope Laboratories, Andover, MA. The PET copolymer resin (IV = 0.72) was obtained from Eastman Chemicals, Kingsport, TN. All the monomers supplied were polymerization grades; therefore they could be used without further purification.

Preparation of PET/MO and PET/CHEDM Copolymers: *In Situ* Polymerization

The batch scale melt polymerization system of RTI Engineering Co., Seoul, South Korea was equipped with an esterification reactor (ES) and a polycondensation reactor (PC) each with a capacity of 3 L. This system was used to prepare PET/MO and PET/CHEDM copolymers by an *in situ* polymerization process. In the first step, TPA and EG were mixed and reacted at 220–245°C under 1 kg_f/cm^2 of N_2 in the ES in order to prepare bishydroxyethyl terephthalate (BHET). Tetramethyl ammonium hydroxide (100 ppm) was added as a diethylene glycol (DEG) suppressor and 1 kg of TPA was used to react with 560 g of EG, so the mole ratio of EG and TPA was 1.5 : 1. During the reaction, the byproduct, which is water, was removed from the reaction mixture. At the end of the esterification reaction, BHET was removed from the reactor.

In the second step, 1250 grams of crushed BHET was dried under vacuum at 130°C overnight, and then melted in the PC at 250°C for 2 h under nitrogen (0.2 kg_f/cm^2 pressure). After BHET was melted, active oxygen scavengers (MO and CHEDM for PET/MO and PET/CHEDM copolymers, respectively), catalyst (antimony trioxide), colorant (cobalt acetate), and a thermal stabilizer (phosphoric acid) were added and then pressurized with N_2. The amounts of additives used for the polycondensation reaction were 250 ppm Sb, 30 ppm Co, 20 ppm P, and 1–5 % (wt/wt) of scavenger with respect to BHET. These were added in the early stage of the polycondensation reaction. These additives were put into the reactor at the same time with stirring and nitrogen flowing to prevent thermo-oxidation. Before their addition, antimony trioxide was mixed with EG and heated up to 150°C for 2 h to form antimony glycolate and cobalt acetate was mixed with hot EG to prepare a solution. The polycondensation reaction was performed at 270–280°C under high vacuum (1–2 torr).

Reaction Analysis

Solution proton nuclear magnetic resonance spectroscopy (^1H NMR) was used to study copolymer synthesis and to evaluate the occurrence of an interchange reaction between PET chains and the scavengers. A 70/30 (wt/wt) d-chloroform/TFA mixture was used to dissolve ground samples for NMR measurements in a high resolution INOVA–600 MHz spectrometer manufactured by Varian Association.

Characterization

Oxygen permeability was determined by measuring the oxygen transmission rate (OTR) at steady state using a whole package MoCon tester. This test is a coulometric method, which follows ASTM D3985 with a test temperature of 23°C and 100% internal relative humidity. The test gas was oxygen at 50% external relative humidity. Sheet samples, with areas of about 8 cm^2, were supported on standard impermeable fixtures with epoxy 53 adherent applied to prevent leaks between the sample sheet and fixture. At steady state equilibrium conditions the OTR was measured by the difference in the partial pressure of oxygen between the two surfaces of the sample according to the following equation.

$$\mathrm{OTR} = (AV - BV) \times \mathrm{IF} = \mathrm{cc\ (STP)/day} \quad (1)$$

where *AV* is the voltage for oxygen permeation in mV, *BV* is the baseline voltage in mV, and IF is an instrument factor which accounts for the cell area and the conversion factor for the detector. Oxygen permeation is the stable value of OTR per unit of oxygen partial pressure difference between the two surfaces. The oxygen permeability is reported as cc(STP)*mil/$100in^2$*day*atm.

Applied Polymer SCIENCE

While improving the oxygen barrier properties of PET is a major goal, it is also important to study scavenger effects in terms of changes in copolymer physical properties in relationship to those of commercially produced unmodified resin. Rheological and thermal properties of the prepared copolymers were evaluated as described below.

The complex melt viscosities (η^*) of dried PET/scavenger copolymer pellets were measured using a parallel disk Rheometric Dynamic Analyzer (RDA III) at 280°C under nitrogen to avoid oxidation and with a gap between the disks of 1 mm. Data for the melt viscosity of pure PET and each copolymer sample were taken at an angular frequency (ω) of 10 rad/s to represent the zero-shear viscosity. This method was used to measure PET samples with known intrinsic viscosity (IV) values (previously determined in 60/40 phenol/tetrachloroethane). The IV results were plotted as functions of ln melt viscosity (PA*s) to obtain the following relationship for IV or (PET equivalent melt IV) and complex viscosity (η^*).

$$\text{IV (Melt IV)} = m \ln(\eta^*) + b \quad (2)$$

Here η^* is the complex viscosity at a frequency of 10 rad/s. The constant m is 0.136 and the value for b is −0.115. PET equivalent melt IV values were calculated for the PET/scavenger copolymer samples using eq. (2) in a manner similar to that described by others.[26–29]

A Perkin–Elmer differential scanning calorimeter model DSC-7, calibrated with indium and zinc standards, was used for thermal analysis of the samples. For these evaluations, pellet samples were ground into powder form and then dried under vacuum for about 12 h at 120°C. Samples were between 5 and 12 mg. In order to remove the previous thermal history of the pure PET and the PET/scavenger copolymer samples, all the samples were quenched very quickly at 300°C/min after their first heating to 300°C. The quenched samples were heated again at 10°C/min to evaluate their glass transition temperatures, crystallization, and melting behaviors. To determine their crystallization behaviors while cooling from the melt, all the samples were cooled at 10°C/min after their second heating. Additional samples were crystallized at various isothermal temperatures after being cooled from the melt.

RESULTS AND DISCUSSION

Synthesis of PET/Scavenger Copolymers

To confirm the occurrence of an interchange reaction between PET and the scavenger (MO and CHEDM) units, NMR spectroscopy measurements were performed on three solutions to obtain: (i) ^{1}H NMR spectrum of pure PET; (ii) ^{1}H NMR spectrum of pure scavenger; and (iii) ^{1}H NMR spectrum of PET/scavenger copolymer. Reaction analysis included in the following discussions have utilized commercially prepared pure PET copolymer resin (IV = 0.72) as well as the copolymer samples of PET/MO and PET/CHEDM prepared through *in situ* polymerization. Figure 1(a) shows the structure of pure PET and its ^{1}H NMR spectrum. The peak at δ = 8.13 ppm is attributed to the protons of the TPA ring of PET and the peak at δ = 4.79 ppm belongs to protons of the EG segment of PET. The other

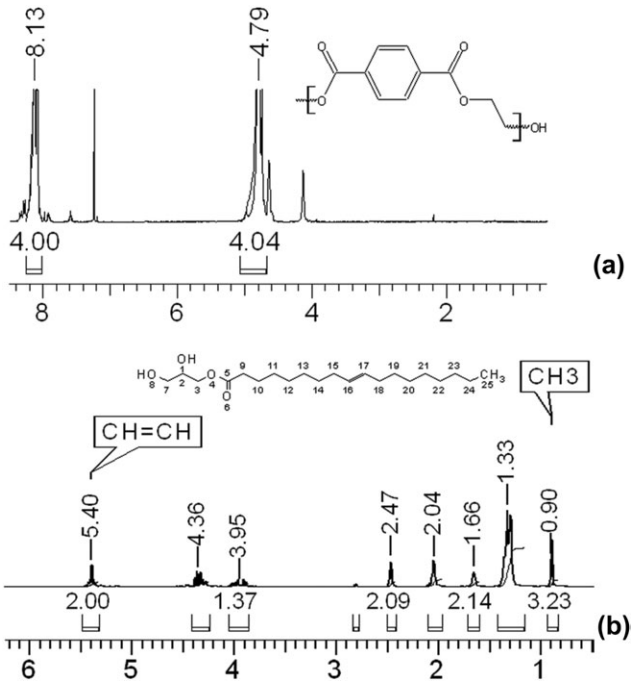

Figure 1. Structures and ^{1}H NMR spectra of (a) pure PET (b) pure MO.

resonances in the range from δ = 4.00 to 4.75 ppm are attributed to the methylene protons of the DEG segment in PET. DEG is formed when two molecules of EG react with each other. During the polymerization process, this DEG can then become part of the PET or PET/scavenger copolymer chain.

Figure 1(b) gives the structure of pure MO and the ^{1}H NMR spectrum of pure MO dissolved in 70/30 (wt/wt) d-chloroform/TFA. Four main peaks appear in the spectrum. The peak at δ = 5.40 ppm belongs to the signal of protons of the double bond (CH═CH) of MO structure. The peaks at δ = 3.95 and 4.2 ppm belong, respectively to the resonances of protons at positions 2 and 7 of MO. The peak at δ = 4.36 ppm is the signal of protons at position 3 of MO structure. Figure 2(a) represents the structure and ^{1}H NMR spectrum of PET/MO (5 wt %) copolymer. Comparing this figure with Figure 1(a,b), it is evident that the peak appearing at δ = 4.78 ppm is the signal of protons of the EG unit of PET/MO copolymer as in the case of the ^{1}H NMR spectrum of pure PET. Peaks appearing between δ = 0.85 and 2.44 ppm are the resonances of the protons of MO in the copolymer as in the case of the ^{1}H NMR spectrum of pure MO. When PET and MO react together, the molecular interaction influences the chemical environment of each component. The chemical shifts of the components in the copolymer should be different from those of their pure state. For PET/MO copolymer [shown in Figure 2(a)], two new signals were found at δ = 5.94 ppm and δ = 4.87 ppm, attributed to the protons of a new copolymer resulting from the interchange reaction between PET and MO. We were however expecting three new signals corresponding to the protons at positions 9, 10, and 20; because PET can react with MO at positions 9 and 20 by replacing —H atom of —OH end groups of MO. These reactions would cause a change in the chemical environment around protons at

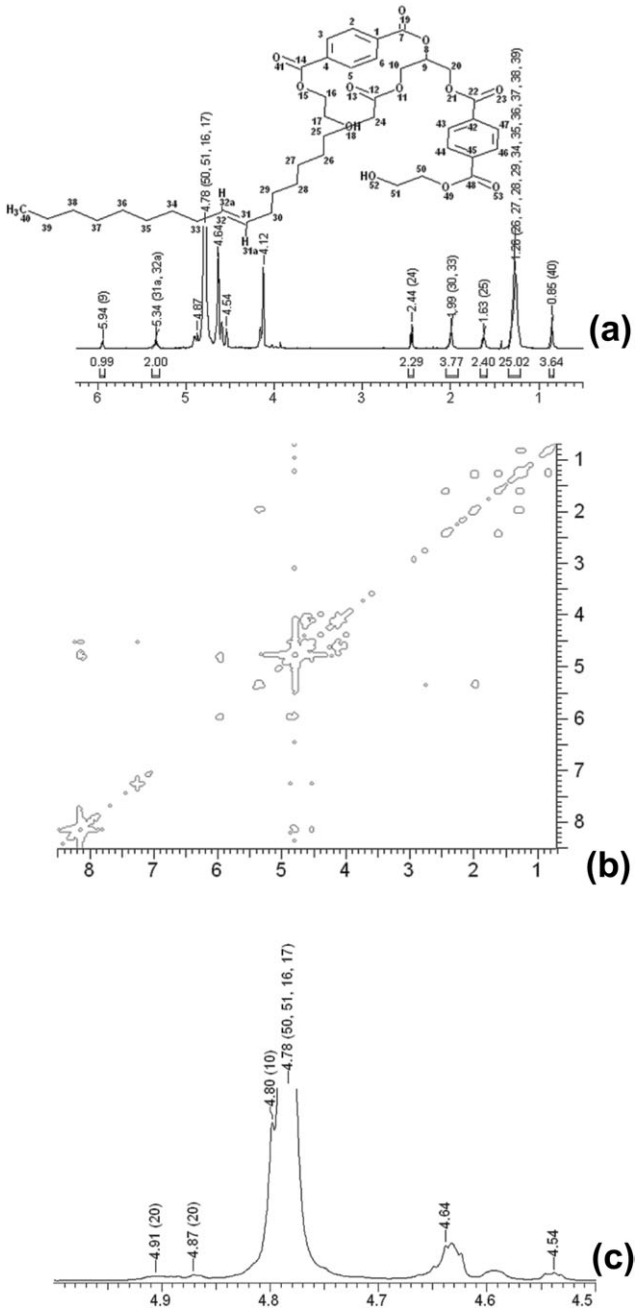

Figure 2. ^{1}H NMR analyses of PET/MO (5 wt %) copolymer showing (a) polymer structure and ^{1}H NMR spectrum, (b) 2D COSY plot, and (c) expanded ^{1}H NMR spectrum.

positions 9, 10, and 20 [shown in Figure 2(a)] and the chemical shift of the protons corresponding to these three positions should be different from that of their pure state.

In order to further substantiate the existence and assignment of the new copolymer peaks, a 2D correlation spectroscopy (COSY) experiment was performed to determine the connectivity of a molecule by determining which protons is spin–spin coupled. In Figure 2(b), the proton spectrum for PET/MO (5 wt %) copolymer is plotted on each of the two axes. The diagonal within the box is also the spectrum for the copolymer as seen from "above". Off-diagonal peaks are denoted through bond coupling between protons on adjacent carbons. The coupling of the proton at $\delta = 5.94$ ppm to the methylene protons (adjacent to position 9 after reaction) at $\delta = 4.8$ ppm and methylene protons at $\delta = 4.87$ ppm. The CH=CH peak at $\delta = 5.34$ ppm is coupled with methylene protons of positions 30 and 33 at $\delta = 1.99$ ppm. The COSY experiment proves that the peak at $\delta = 5.94$ ppm has four cross-peaks between $\delta = 4.8$ and 4.9 ppm and among these four peaks, the two important cross-peaks appear at $\delta = 4.80$ and 4.87 ppm. This means that the peak corresponding to $\delta = 5.94$ ppm is directly connected to these two cross-peaks. This leads us to conclude that the two cross-peaks correspond to protons of positions 10 and 20. The expanded spectrum in Figure 2(c) shows the two new peaks at $\delta = 4.80$ and 4.87 ppm.

During initial measurement of pure CHEDM in a 70/30 (wt/wt) d-chloroform/TFA, three main peaks appeared in the ^{1}H NMR spectrum. The first main peak between $\delta = 3.78$ ppm and $\delta = 4.35$ ppm belonged to the signal of protons at positions 7 and 9 of the CHEDM structure. The chemical environment of protons at positions 7 and 9 is very similar; therefore they should have given one rather than two peaks. Figure 3(a) gives the CHEDM structure and also illustrates the ^{1}H NMR spectrum of pure CHEDM after it had been dissolved in the solvent for 1 day. Peaks corresponding to protons at positions 7 and 9, which were previously at $\delta = 3.78$ and $\delta = 4.35$ ppm, have emerged as one peak now and appear at $\delta = 4.34$ ppm. This may have occurred because the first NMR spectrum was obtained using a freshly prepared sample and the —CH_2 groups of pure CHEDM were still moving, when dissolved in solvent. After the sample

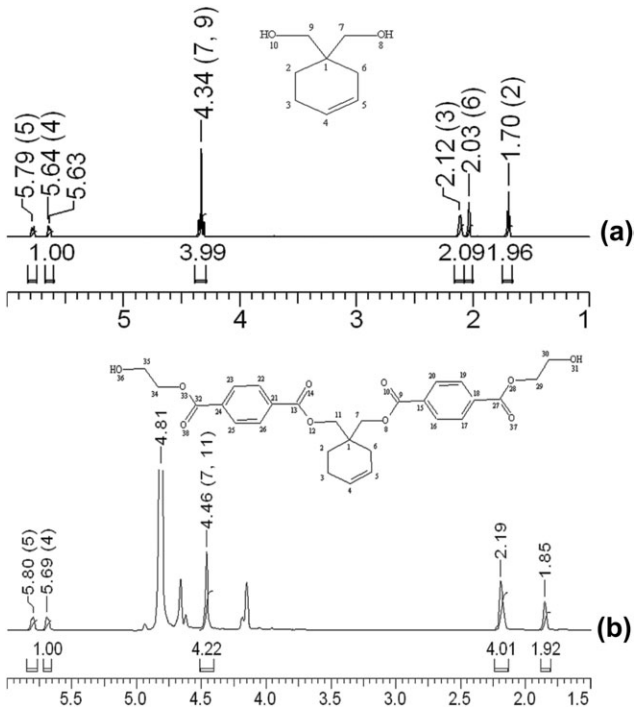

Figure 3. Structures and ^{1}H NMR spectra of (a) pure CHEDM after 1 day and (b) PET/CHEDM (5 wt %) copolymer.

Applied Polymer SCIENCE

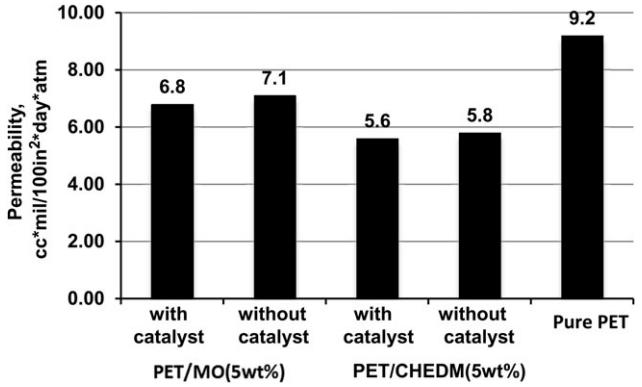

Figure 4. Average oxygen permeability values for PET/MO and PET/CHEDM copolymers (prepared with and without catalyst) and for pure PET.

was held in the solvent for one day, the —CH_2 groups had sufficient time to relax and therefore they appear as one peak. The second main peak at $\delta = 5.75$ ppm belongs to the resonance of the proton at position 5 of the CHEDM structure. The third main peak at $\delta = 5.62$ ppm is associated with the proton at position 4 of the CHEDM structure. The peaks between $\delta = 1.88$ and 2.07 ppm are the signals of protons of positions 2, 3, and 6 of the CHEDM structure. In addition, it was seen in Figures 3(a) that peaks between $\delta = 1.88$ and 2.07 ppm also changed their chemical shifts with longer time in solution. This may have resulted from hydrogen bonding between the d-TFA and CHEDM molecules.

Figure 3(b) represents the expected structure and ^{1}H NMR spectrum of a PET/CHEDM (5 wt %) copolymer. Comparing Figure 3(b) with Figures 1(a) and 3(a), it is evident that the peak appearing at $\delta = 4.81$ ppm is the signal of protons of the EG unit of PET/CHEDM copolymer as in the case of the ^{1}H NMR spectrum of pure PET. Peaks appearing at $\delta = 1.85$ ppm, and $\delta = 2.19$ are the resonances of the protons of CHEDM in the copolymer as in the case of the ^{1}H NMR spectrum of pure CHEDM. When PET and CHEDM react, the molecular interaction influences the chemical environment of each component. The interchange reaction leads to the formation of a new copolymer. For a PET/CHEDM copolymer, we find new signals attributed to the protons of a new copolymer, which are the product of the interchange reaction between the PET and CHEDM units [shown in Figure 3(b)]. The peak at $\delta = 4.46$ ppm is attributed to the new chemical shift for protons of positions 7 and 11, which was at $\delta = 4.34$ ppm in the ^{1}H NMR spectrum of pure CHEDM. The protons at positions 4 and 5 have similar chemical shifts of $\delta = 5.69$ and $\delta = 5.80$ ppm, respectively, as in the ^{1}H NMR spectrum of pure CHEDM, because this group is quite far from the position where the reaction has occurred. The areas under the peaks at $\delta = 5.69$ and $\delta = 5.80$ ppm are each '1' and the area under the peak at $\delta = 4.46$ ppm is about '4'. This ratio should be 1 : 1 : 4, respectively, because the positions 4 and 5 have '1' proton each and the positions 7 and 11 have '4' protons in total. The areas under the peaks satisfy this ratio.

Oxygen Permeability

Oxygen barrier properties of extruded copolymer sheets samples, containing 5% of each scavenger, were evaluated using a whole package MoCon tester. In order to enhance oxygen uptake and improve the rate of reaction between the scavengers and permeating oxygen, cobalt octoate catalyst was added to portions of the dried copolymer pellets just before sheet extrusion. Figure 4 shows the average permeability values obtained for pure PET, PET/MO (5 wt %) and PET/CHEDM (5 wt %) copolymer sheets, both with and without catalyst. It can be seen that the average permeability values for the PET is 9.2 cc*mil/100in^2*day*atm. Those for the MO samples are 6.8 and 7.1 cc*mil/100in^2*day*atm. and for the CHEDM samples 5.6 and 5.8 cc*mil/100in^2*day*atm., with slightly lower values recorded in the presence of catalyst. In comparison to the commercial PET, there are improvements of almost 30 and 40% in the respective PET/MO and PET/CHEDM copolymer oxygen permeability values.

Rheological Behavior of PET/Scavenger Copolymers

Figure 5(a) illustrates the complex viscosity (η^*) (melt viscosity) of a commercial PET copolymer sample plotted as a function of angular frequency (which can be taken as a measure of shear rate). It is evident that the PET sample shows Newtonian behavior within the measured frequency values. This is typical of rheological behavior observed for pure PET. Figure 5(a) also illustrates changes in η^* as a function of frequency, measured for copolymer samples with 1 and 5 wt % MO. The copolymer

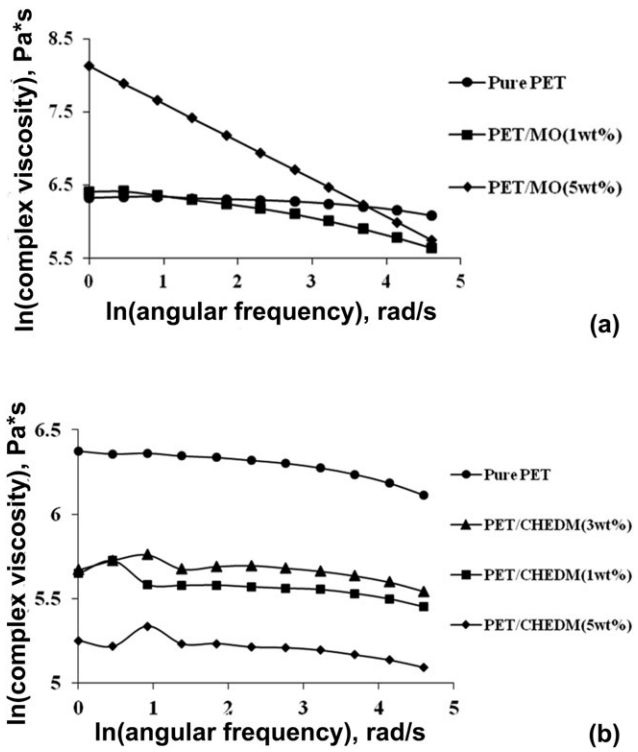

Figure 5. Rheological properties using RDA of [shear viscosity] complex melt viscosity (η^*) versus angular frequency(ω) for (a) Pure PET and PET/MO copolymers with 1 and 5 wt % MO and (b) for PET/CHEDM copolymers with 0, 1, 3, and 5 wt % CHEDM and Pure PET.

Table I. Melt IV Values Calculated for Pure PET, PET/MO and PET/CHEDM Copolymers at Shear Rates of 10/sec

Material	Melt IV[a]
Pure PET copolymer	0.73
1 wt % MO, PET/MO copolymer	0.72
5 wt % MO, PET/MO copolymer	Non-Newtonian
1 wt % CHEDM, PET/CHEDM copolymer	0.63
3 wt % CHEDM, PET/CHEDM copolymer	0.63
5 wt % CHEDM, PET/CHEDM copolymer	0.58

[a]PET, Equivalent melt IV.

sample of PET/MO (1 wt %) shows Newtonian behavior up to low frequency values, similar to that of pure PET. The copolymer sample of PET/MO (5 wt %), however, shows non-Newtonian behavior even at low frequencies. This behavior is consistent with the formation of branching among the PET and the MO chains.

Complex viscosity values obtained for the copolymer samples of PET/CHEDM and pure PET at 280°C are presented as functions of frequency in Figure 5(b). It should be noted that the copolymer samples of PET/CHEDM with three different compositions of CHEDM (1, 3, and 5 wt %) show Newtonian behaviors at the measured frequencies, similar to behavior of pure PET.

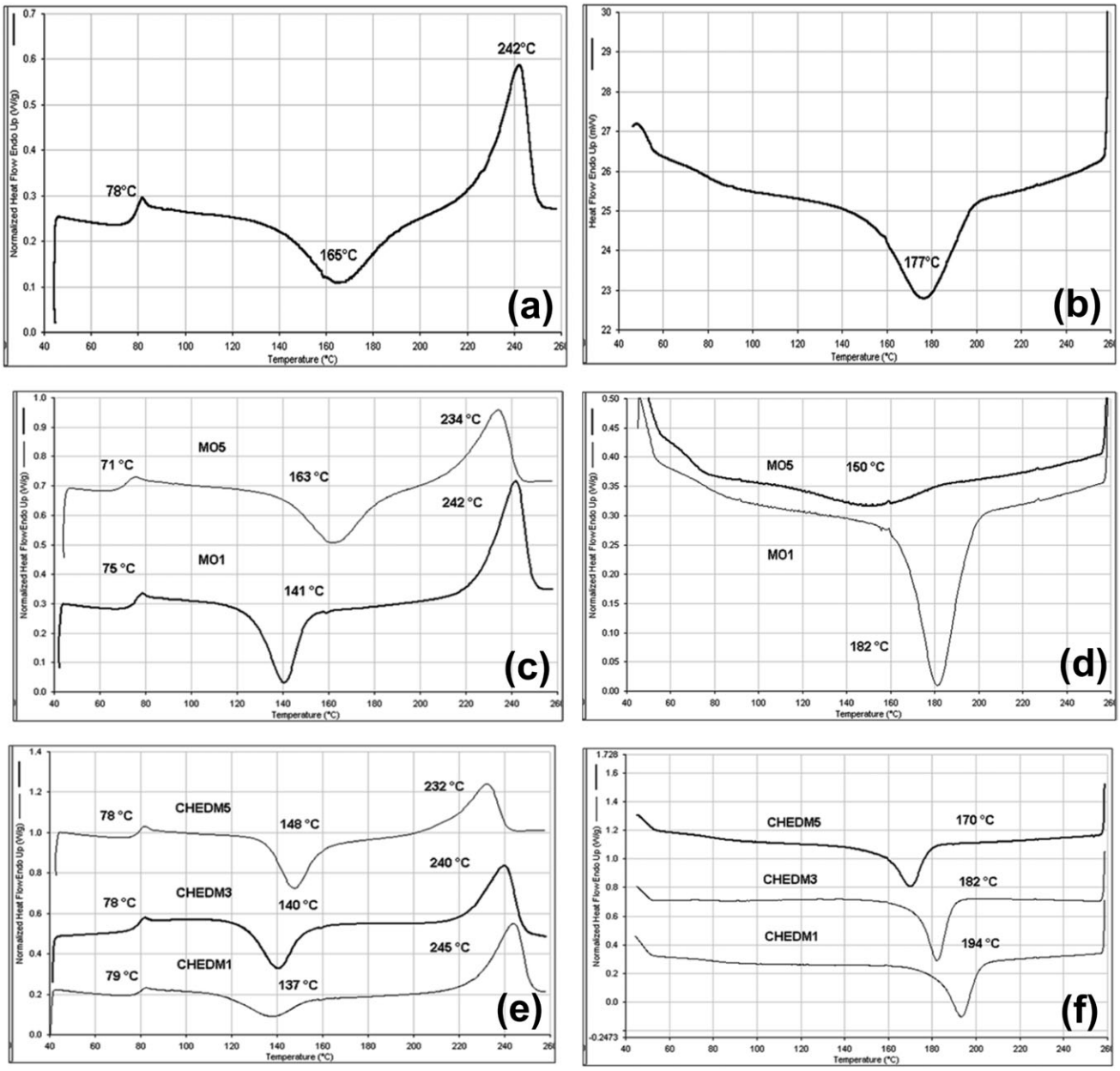

Figure 6. DSC thermograms obtained at heating and cooling rates of 10°C/min showing (a) reheating of amorphous PET, (b) cooling PET from the melt, (c) reheating of amorphous PET/MO copolymer samples, (d) cooling PET/MO copolymer samples from the melt, (e) reheating of amorphous PET/CHEDM copolymer samples, and (f) cooling PET/CHEDM copolymer samples from the melt.

Table II. Thermal Data Collected from DSC Thermographs of PET/MO Copolymers

PET/MO copolymers	Heating from the quench					Cooling from the melt
	Melting			Crystallization		Crystallization
	T_g (°C)	T_m (°C)	ΔH_m (J/g)	T_c (°C)	ΔH_c (J/g)	T_{cc} (°C)
1 wt % MO	75	242	33	141	−28	182
5 wt % MO	71	234	28	163	−27	150

Table I gives PET equivalent melt IV rheology results obtained for PET and the copolymers.

Thermal Analysis of PET/scavenger Copolymers

The influences of the interchange reactions on the melting behaviors and the morphologies of the PET/scavenger copolymers have also been investigated. Thermal properties are important because they dictate the processing conditions, for injection molding and stretch blow molding, needed for a particular resin. Changes in the glass transition temperature (T_g), crystallization behavior, and melting behavior were evaluated for PET and both MO and CHEDM copolymer samples. The isothermal and nonisothermal crystallization behaviors of the PET/scavenger copolymer samples were studied as functions of the types and contents of the scavengers.

The DSC thermograms of pure PET are shown in Figure 6(a,b). The glass transition temperature is 78°C, the crystallization peak temperature is 165°C, and the peak melting point of pure PET is 242°C [Figure 6(a)]. Figure 6(b) shows the crystallization behavior of pure PET as it is cooled from the melt at 10°C per minute. The melting and crystallization behaviors of the PET/scavenger copolymer samples should not be directly compared with those of pure PET, because the PET is a commercially prepared SSP resin with a different synthesis and processing history.

The DSC thermograms of PET/MO copolymers, shown in Figure 6(c), indicate that the glass transition temperature of the copolymer of PET with 1 wt % MO is 75°C and with 5 wt % MO is 71°C. The data for 1 wt % and 5 wt % MO indicate an increase in crystallization temperature with increasing MO content. This means that a higher MO content reduces the copolymer's tendency to crystallize when heating from the quenched amorphous state. In addition to the increase in crystallization temperature, the melting point of the copolymer decreases with increasing MO content in the range of 1–5 wt %, enabling the PET/MO copolymers to be processed at lower temperatures than a PET homopolymer. PET/MO copolymers have melting points of 242°C for 1 wt % MO and 234°C for 5 wt % MO. Figure 6(d) shows the crystallization behavior of the PET/MO copolymer samples upon cooling from the melt at 10°C per minute. It is evident that the crystallization peak temperature (T_{cc}) and level of crystallinity achieved, decreases as MO content increases in the copolymer. This is consistent with the crystallization behavior observed while reheating after quenching. These results are summarized in Table II.

The DSC thermograms of PET/CHEDM copolymers, shown in Figure 6(e), indicate that the glass transition temperatures of the copolymer of PET with 1, 3, and 5 wt % CHEDM are 79, 78, and 78°C, respectively. The crystallization data for these samples show increases in crystallization temperature with increasing comonomer (CHEDM) content in the copolymer indicating that the higher the CHEDM content in the copolymer, the slower is the crystallization. In addition to the increase in crystallization temperature, the melting points of the copolymers decrease with increasing CHEDM content in the range of 1–5 wt %, enabling the PET/CHEDM copolymers to be processed at lower temperatures than PET homopolymer. PET/CHEDM copolymers have lower melting points (T_m = 245°C for 1 wt % CHEDM, T_m = 240°C for 3 wt % CHEDM, and T_m = 232°C for 5 wt % CHEDM). The depression of melting temperature could be attributed to the transesterified CHEDM units which restrict PET crystallization, and reduce PET crystallite size. It may also be caused by the broadening of the interfacial region from the introduction of the CHEDM block. Figure 6(f) shows the crystallization behavior of the PET/CHEDM copolymer samples upon cooling from the melt at 10°C per minute. It is evident that the crystallization temperatures (T_{cc}) decrease as CHEDM contents increase in the copolymers. This is consistent with the crystallization behavior observed while reheating quenched samples. These data are summarized in Table III.

Table III. Thermal Data Collected from DSC Thermographs of PET/CHEDM Copolymers

PET/CHEDM copolymers	Heating from the quench					Cooling from the melt
	Melting			Crystallization		Crystallization
	T_g (°C)	T_m (°C)	ΔH_m (J/g)	T_c (°C)	ΔH_c (J/g)	T_{cc} (°C)
1 wt % CHEDM	79	245	32	137	−19	194
3 wt % CHEDM	78	240	32	140	−28	182
5 wt % CHEDM	78	232	26	148	−27	170

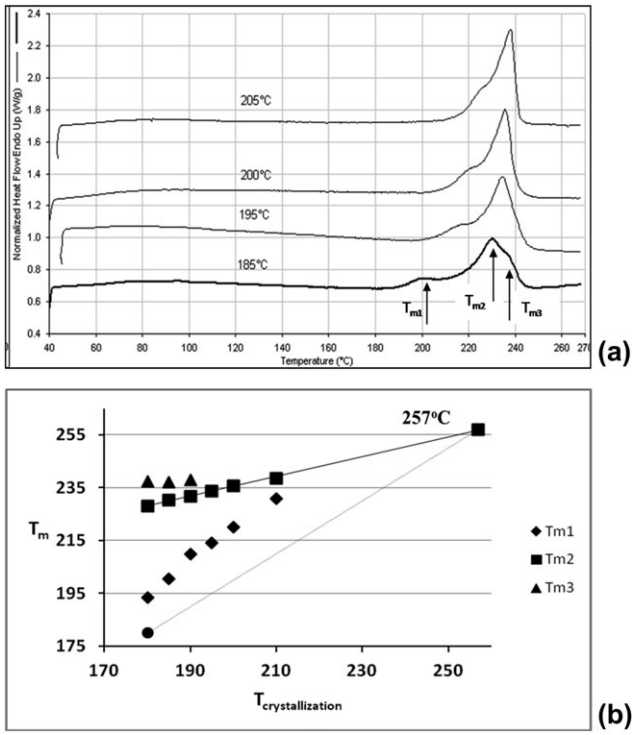

Figure 7. (a) DSC thermograms obtained at heating rates of 10°C/min showing multiple melting peaks of PET/MO (5 wt %) copolymer samples, isothermally crystallized at the indicated temperatures and (b) an example of plots used to obtain the equilibrium melting temperature (T_m^o) of PET/MO (5 wt %) copolymer.

To study the isothermal crystallization kinetics of the copolymers, crystal growth analysis was done. There have been many attempts to develop theories to explain the important aspects of crystallization.[30,31] The most widely accepted approach to the analysis of the crystal growth rates is the kinetic description of Lauritzen and Hoffmann [30]. The general expression of crystal growth as described by Lauritzen and Hoffman is:

$$G = G_0 \exp(-U^*/R\,(T_c - T_\infty)) \exp(-K_g/T_c \Delta T f) \quad (3)$$

Where

G = growth rate
G_0 = growth rate constant
U^*= activation energy for polymer diffusion
R = gas constant
T_c = crystallization temperature (°K)
$T_\infty = T_g - 30$ (°K)
ΔT = degree of undercooling = $T_m^o - T_c$
T_m^0 = equilibrium melting temperature (°K)
f = correction factor
K_g = nucleation rate constant

From eq. (3), it is clear that the crystal growth rate is dependent on the degree of undercooling and nucleation rate constant. The nucleation rate constant is further dependent on the equilibrium melting temperature (T_m^o). Therefore, the determination of T_m^o and degree of undercooling (ΔT) is essential to study the isothermal crystallization kinetics of the PET/scavenger copolymers. The equilibrium melting point is obtained through extrapolative procedures. Two general methods have been devised for the evaluation of equilibrium melting points of semicrystalline polymers: the Hoffmann-Weeks[32] and the Gibbs–Thomson procedures.[33] In order to determine their equilibrium melting points (T_m^o), samples were crystallized at various temperatures for 1 h.

Equilibrium Melting Point

Figure 7(a) shows an example of the multiple melting peaks[34] obtained for PET/MO (5 wt %) copolymer samples. Isothermal crystallization temperatures are noted on the respective melting curves of each figure. An isothermally crystallized PET/MO (5 wt %) copolymer sample exhibits three melting peaks identified as T_{m1}, T_{m2}, and T_{m3} in Figure 6(a). Isothermal crystallization temperatures were from 180 to 220°C. Other isothermally crystallized copolymer samples of PET/MO, PET/CHEDM, and pure PET also showed three melting peaks. Although there are many different interpretations about the phenomena of multiple melting peaks, it is generally accepted that the melting peak T_{m1} is associated with the melting of crystals formed in secondary crystallization, the melting peak T_{m2} is due to the melting of crystals formed in primary crystallization, and the melting peak T_{m3} is related with the melting of crystals formed from reorganization during heating.[32,33]

The three melting peaks seen in Figure 7(a) are related to the melting of crystalline components in the PET/MO (5 wt %) copolymer sample. With increasing isothermal crystallization temperatures, the positions of T_{m1} and T_{m2} shift to higher temperatures and the position of T_{m3} does not change. If we plot melting temperature (T_{m2}) versus T_c and extrapolate the T_{m2} line to higher temperatures, it will intercept with a theoretical line constructed from equivalent melting and crystallization temperatures. According to the method of Hoffman and Weeks,[30,32] this intercept is the equilibrium melting point (T_m^o) of the evaluated material. Figure 7(b) shows an example of the plots used for the calculation of T_m^o for the PET/MO (5 wt %) copolymer. Similar plots were constructed for other copolymer samples and pure PET. Results of these evaluations are summarized in Table IV. As can be seen the equilibrium melting point (T_m^o) is depressed with increasing MO and CHEDM contents.

Crystallization Kinetics

In addition to the melting behavior, the crystallization behavior observed while the samples were isothermally crystallized at

Table IV. Equilibrium Melting Points of PET/MO and PET/CHEDM Copolymers, and Pure PET

Material	Scavenger (wt %)	T_m^o (°C)
Pure PET	0	257
PET/MO copolymer	1	263
	5	257
PET/CHEDM copolymer	1	267
	3	264
	5	255

Applied Polymer SCIENCE

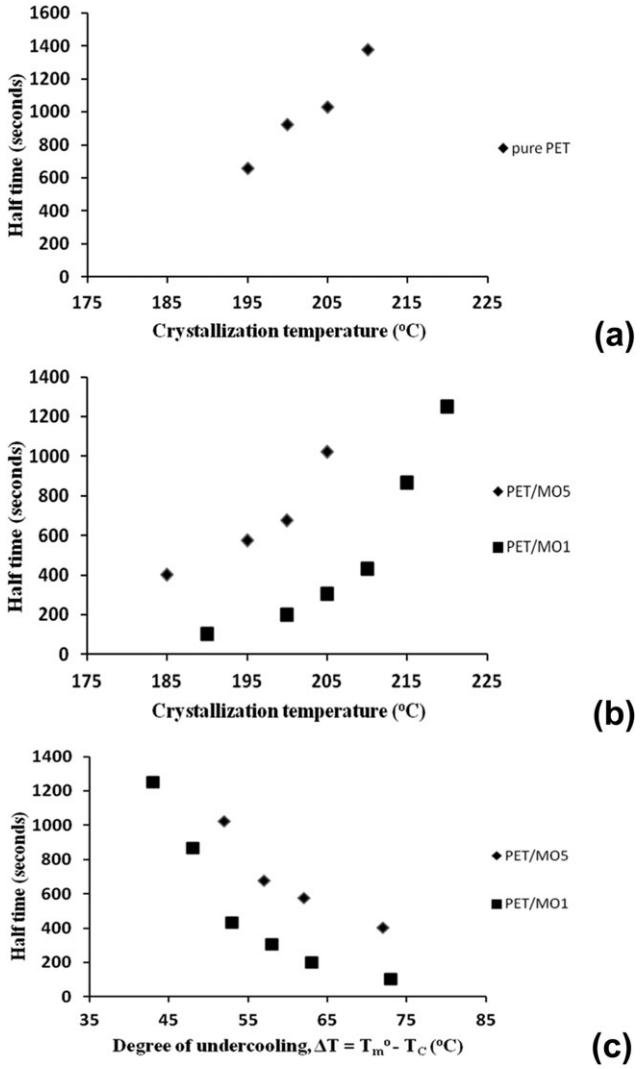

Figure 8. Half times of crystallization plotted as functions of crystallization temperatures for isothermally crystallized (a) pure PET, (b) PET/MO copolymer samples, and (c) half times plotted as functions of degrees of undercooling for PET/MO copolymer samples.

various temperatures was also examined. Data recorded for these samples have been evaluated in terms of each material's crystallization half time, which is the time at which the relative crystallinity of the polymers achieves 50% of the total crystallinity measured at that temperature and can reflect the overall crystallization rate of the polymers. In Figures 8 and 9, the crystallization behaviors of pure PET and the PET/scavenger copolymers are displayed in terms of their crystallization half times. From Figures 8(a,b), it is evident that as the crystallization temperature of pure PET and PET/MO copolymers increases, the half time also increases. It can also be observed that as the concentration of MO increases, the half time increases. These results are consistent with the nonisothermal crystallization behavior for PET/MO copolymers, indicating that the higher the MO content in the copolymer the slower is the crystallization.

The true driving force of crystallization of polymers is the degree of undercooling. This is the difference between the equilibrium

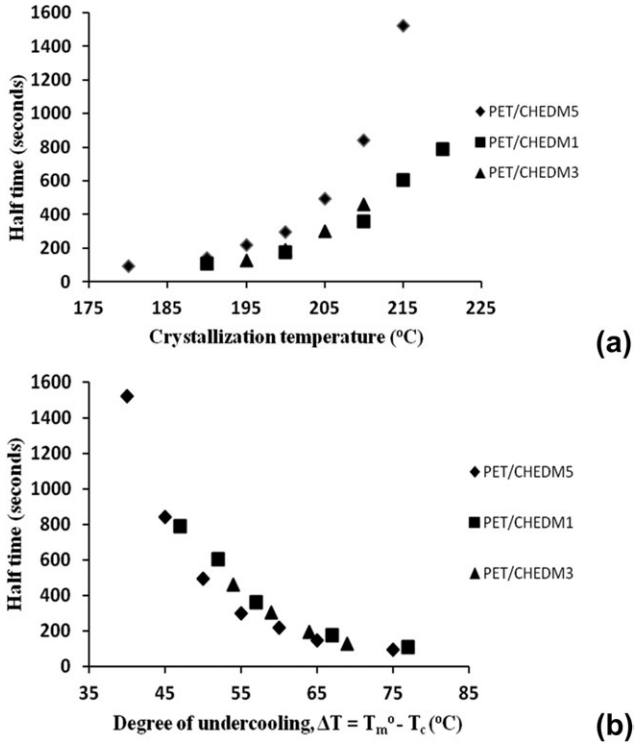

Figure 9. (a) Half times of crystallization plotted as functions of crystallization temperatures for isothermally crystallized PET/CHEDM copolymer samples and (b) half times plotted as functions of degrees of undercooling for PET/CHEDM copolymer samples.

melting point (T_m^o) of the polymers and the crystallization temperature (T_c). The degree of undercooling is important because the equilibrium melting points of the PET/scavenger copolymers are different. The crystallization data should be more meaningful if the results of the crystallization half times for different copolymer samples are compared at the same degrees of undercooling.

Figure 8(c) illustrates a plot of the half times as functions of their degrees of undercooling for the PET/MO copolymer samples. As the MO content increases in the copolymer, the crystallization half time also increases at the same degree of undercooling, indicating that the crystallization rate of the PET/MO copolymer decreases.

The PET/CHEDM copolymer samples were treated in a manner similar to that described for the PET/MO copolymer samples. From Figure 9(a), it can be seen that as the CHEDM content increases, the half time also increases when the samples are crystallized at the same crystallization temperature (especially at higher crystallization temperatures). This means that the higher the CHEDM content, the slower is the crystallization. Figure 9(b) illustrates the relationship of their half times as functions of degrees of undercooling for the PET/CHEDM copolymer samples and indicates that in this case there are no significant differences in the crystallization behaviors for PET/CHEDM copolymer samples with different concentrations of CHEDM.

In addition to the half time analyses, the previously discussed data were also used to determine crystallization kinetics in terms of the Avrami expression given by:

Table V. Avrami n and k Values for PET/Scavenger Copolymer Samples and Pure PET

Isothermal crystallization temperature (°C)	Avrami Parameters	Pure PET	PET/MO (1 wt %)	PET/MO (5 wt %)	PET/CHEDM (1 wt %)	PET/CHEDM (3 wt %)	PET/CHEDM (5 wt %)
180	n	-	-	-	-	-	7.0
	k (sec^{-n})	-	-	-	-	-	1.9×10^{-14}
185	n	-	-	2.7	-	-	-
	k (sec^{-n})	-	-	7.9×10^{-8}	-	-	-
190	n	-	-	-	-	-	6.5
	k (sec^{-n})	-	-	-	-	-	1.2×10^{-14}
195	N	2.5	-	2.5	-	6.5	6.0
	k (sec^{-n})	9.8×10^{-8}	-	8.0×10^{-8}	-	2.4×10^{-14}	9.3×10^{-15}
200	n	2.5	-	2.1	2.9	5.6	5.9
	k (sec^{-n})	3.7×10^{-8}	-	7.9×10^{-7}	3.4×10^{-7}	2.1×10^{-13}	2.9×10^{-15}
205	n	2.4	3.0	2.0	-	6.2	6.0
	k (sec^{-n})	5.2×10^{-8}	2.4×10^{-8}	5.0×10^{-7}	-	8.2×10^{-16}	6.2×10^{-17}
210	n	2.2	2.6	-	2.4	5.6	6.0
	k (sec^{-n})	8.0×10^{-8}	9.1×10^{-8}	-	6.9×10^{-7}	2.0×10^{-15}	2.2×10^{-18}
215	n	-	2.5	-	2.4	-	6.4
	k (sec^{-n})	-	4.4×10^{-8}	-	1.6×10^{-7}	-	5.3×10^{-21}
220	n	-	2.7	-	2.5	-	-
	k (sec^{-n})	-	3.0×10^{-9}	-	3.7×10^{-8}	-	-

$$\theta_a = e^{-kt^n} \tag{4}$$

Where θ_a is the fraction of uncrystallized material, k is the kinetic rate constant, t is the time, and n is the Avrami exponent, describing the mechanism of crystallization. The mathematical formulation of the kinetic phase change and the derivation of the Avrami equation can be found elsewhere.[35] In the Avrami expression, the kinetic rate constant (k) is a function of the nucleation and the growth rates, while the Avrami exponent (n) provides qualitative information on the nature of nucleation and the growth processes. Values of (n) generally range from 1 to 4, for various types of nucleation and growth.[36,37] The kinetic parameters from eq. (4) are obtained by plotting the data according to eq. (5).

$$\ln(-\ln \theta_a) = \ln\ k + n\,(\ln\ t) \tag{5}$$

A plot of ln (-ln θ_a) versus ln t yields a straight line with the slope equal to n and the intercept equal to ln k.

The crystallization data recorded for pure PET, PET/MO copolymers, and PET/CHEDM copolymers were used to plot (θa) values as functions of crystallization times (ln t). These isotherms all exhibited the sigmoidal shapes typical of polymer crystallization behavior. For the same crystallization times, as crystallization temperatures increased, fractions of uncrystallized material also increased. Avrami plots were also constructed according to eq. (5); with ln (–ln θa) values plotted as functions of ln t. Slopes and intercepts of the straight lines obtained were used to calculate values for n and k. For these calculations; however, only initial portions of the crystallization data were used in order to obtain values for primary crystallization. During secondary crystallization,[38–40] different slopes are observed and values for n are reduced.

Table V summarizes the n and k values obtained during primary crystallization of pure PET and the PET/MO and PET/CHEDM copolymer samples. These results show that the Avrami exponent (n) values for pure PET, PET/MO (1 and 5 wt %), and PET/CHEDM (1 wt %) copolymer samples, vary between 2 and 3, indicating spherulitic growth from instantaneous nuclei. This conclusion is corroborated by additional work (not included) with polarized light microscopy and small angle light scattering that clearly shows the presence of spherulitic structures.[41] The n values obtained for the copolymer samples containing 3 and 5 wt % CHEDM are near 6 and outside the expected range. Similar high values have been reported by others and attributed to numerous small particles with high surface energies that acted as nucleating agents.[42]

Half-Life Method

Application of the Avrami kinetics gave unusually high n values for copolymer samples containing 3 and 5 wt % CHEDM; therefore, the half-life (half time) method[36] was applied to calculate all the n and k values. This method has been reported by other researchers,[43] to be more accurate for analysis of some polymers. These calculations utilized the previously described data with θa values plotted as functions of ln t. At the half time ($t_{1/2}$) of each plot (θa = 0.5) the slope (S) was taken and used to calculate (n) according to eq. (6)

$$S = -0.35^{*} n \tag{6}$$

Table VI. Avrami n and k Values for PET and PET/Scavenger Copolymers using the Half-Life Method

Isothermal crystallization temperature (°C)	Avrami Parameters	Pure PET	PET/MO (1 wt %)	PET/MO (5 wt %)	PET/CHEDM (1 wt %)	PET/CHEDM (3 wt %)	PET/CHEDM (5 wt %)
180	n	-	-	-	-	-	3.5
	k (sec^{-n})	-	-	-	-	-	7.2×10^{-8}
185	n	-	-	2.0	-	-	-
	k (sec^{-n})	-	-	3.5×10^{-6}	-	-	-
190	n	-	-	-	-	-	3.0
	k (sec^{-n})	-	-	-	-	-	2.2×10^{-7}
195	n	1.6	-	2.0	-	3.6	2.8
	k (sec^{-n})	2.2×10^{-5}	-	1.8×10^{-6}	-	2.3×10^{-8}	2.1×10^{-7}
200	n	1.6	-	1.9	2.1	3.7	2.6
	k (sec^{-n})	1.5×10^{-5}	-	2.9×10^{-6}	1.1×10^{-5}	4.0×10^{-9}	3.5×10^{-7}
205	n	1.6	2.3	2.0	-	3.6	3.3
	k (sec^{-n})	9.1×10^{-6}	1.1×10^{-6}	6.2×10^{-7}	-	1.0×10^{-9}	7.4×10^{-10}
210	n	1.8	2.1	-	2.0	3.4	3.1
	k (sec^{-n})	1.4×10^{-6}	2.1×10^{-6}	-	4.2×10^{-6}	8.0×10^{-10}	4.5×10^{-10}
215	n	-	2.1	-	1.9	-	3.9
	k (sec^{-n})	-	4.7×10^{-7}	-	3.4×10^{-6}	-	3.3×10^{-13}
220	n	-	2.3	-	2.3	-	-
	k (sec^{-n})	-	7.4×10^{-8}	-	1.5×10^{-7}	-	-

The n and $t_{1/2}$ values (seconds) were then substituted into eq. (7) to obtain k.

$$k = 0.69/{t_{1/2}}^{n} \tag{7}$$

This method monitors behavior that could include primary and the initial portion of secondary crystallization. As a result these n values are lower in most cases and more reasonable for the copolymer samples containing 3 and 5 wt % CHEDM. A summary of the n and k values for the crystallization behavior of the PET, PET/MO, and PET/CHEDM copolymer samples determined by the half-life method is given in Table VI. These n values vary from 1.6 to 2.3 (average 2.0) for the PET, copolymer samples of PET/MO (1 and 5 wt %), and PET/CHEDM (1 wt %). In the case of copolymer samples containing 3 and 5 wt % CHEDM the n values range from 2.6 to 3.9 with an average of 3.3. As reported by others,[44,45] these results indicate that the crystallization mechanism are somewhat different for the MO and CHEDM copolymers.

CONCLUSIONS

PET copolymers were synthesized with MO and CHEDM scavengers at different concentrations, at temperatures between 270 and 280°C, using a batch scale melt polymerization system. ^{1}H NMR spectroscopy and 2D COSY experiments proved that there was an interchange reaction between PET and the MO units as well as between PET and the CHEDM units during polymerization leading to the formation of PET/scavenger copolymers. The oxygen barrier properties of scavenger containing copolymers improved by up to 40%; in comparison to unmodified commercial PET. The T_g and T_m of the PET/MO copolymers decreased as the MO contents increased from 1 to 5 wt %. This decrease resulted from the long side chains of MO in the copolymer. The T_g values of the PET/CHEDM copolymers did not change as the CHEDM content was increased from 1 to 5 wt %; however, the melting peak temperatures (T_m) were found to decrease. The depression of melting temperature could be attributed to the transesterified CHEDM units which restrict PET crystallization, and reduce PET crystallite size. Crystallization rates of the PET/MO copolymers were reduced as the MO content in the copolymer increased from 1 to 5 wt %. Similar crystallization behavior was observed for the PET/CHEDM copolymers, as CHEDM contents in the copolymers increased from 1 to 5 wt %. Pure PET showed Newtonian rheological behavior within the measured range of shear rates, as did the PET copolymer sample with 1 wt % MO. The copolymer sample with 5 wt % MO, however, showed non-Newtonian behavior even at low shear rates. The copolymer samples of PET/CHEDM with three different compositions of CHEDM showed Newtonian behavior at the measured shear rates, in a manner similar to that of PET. The equilibrium melting points (T_m^o) of the copolymers were depressed with increasing MO and CHEDM contents in the copolymers. Crystallization kinetic parameters (n and k) determined by the Avrami expression and half time method indicated that the crystallization mechanisms were different for the MO and CHEDM copolymer samples.

ACKNOWLEDGMENTS

The authors gratefully acknowledge the Chemical and Environmental Engineering Department of The University of Toledo and the Active Barrier Consortium for their kind support of this research.

REFERENCES

1. Jabarin, S. A. Polymeric Materials Encyclopedia; CRC: Boca Raton, FL, Editor Joseph C. Salamone, **1996**, Vol.*8*, 6091.
2. Natu, A. A.; Lofgren, E. A.; Jabarin. S.A. *Polym. Eng. Sci.* **2005**, *45*, 400.
3. Lin, J.; Shenogin, S.; Nazarenko, S. *Polymer* **2002**, *43*, 4733.
4. Qureshi, N.; Stepanov, E. V.; Schiraldi, D.; Hiltner, A.; Baer, E. *J. Polym. Sci. Part B: Polym. Phys.* **2000**, *38*, 1679.
5. Polyakova, A.; Conner, D. M.; Collard, D. M.; Schiraldi, D. A.; Hiltner, A.; Baer, E. *J. Polym. Sci. Part B: Polym. Phys.* **2001**, *39*, 1900.
6. Polyakova, A.; Liu, R. Y. F.; Schiraldi, D. A.; Hiltner, A.; Baer, E. *J. Polym. Sci. Part B: Polym. Phys.* **2001**, *39*, 1889.
7. Polyakova, A.; Stepanov, E. V.; Sekelic, D.; Schiraldi, D. A.; Hiltner, A.; Baer, E. *J. Polym. Sci. Part B: Polym. Phys.* **2001**, *39*, 1911.
8. Hu, Y. S.; Prahipati, V.; Mehta, S.; Schiraldi, D. A.; Hiltner, A.; Baer, E. *Polymer* **2005**, *46*, 2685.
9. Callander, D. D., In Chapter 9 in Modern Polyesters: Chemistry and Technology of Polyesters and Copolymers; Scheirs, J., Long, T. E., Eds.; John Wiley & Sons Ltd., England, **2003**.
10. Wen, J.; Mark, J. E. *J. Mater. Sci.* **1994**, *29*, 499.
11. Pu, Z.; Mark, J. E.; Jethmalani, J. M.; Ford, W. T. *Polym. Bull.* **1996**, *37*, 545.
12. Hajji, P.; Cavaille, J. Y.; Favier, V.; Gauthier, C.; Vigier, G. *Polym. Comp.* **1996**, *17*, 612.
13. Frisch, H. L.; Mark, E. J. *Chem. Mater.* **1996**, *8*, 1735.
14. Kim, S. G. Ph.D. Thesis, Polymer Institute, University of Toledo, **2007**.
15. Labde, R. Master's Thesis, Polymer Institute, University of Toledo, **2010**.
16. Chang, J. H.; Park, D. K. *Polym. Bull.* **2001**, *47*, 191.
17. Saujanya, C.; Imai, Y.; Tateyama, H. *Polym. Bull.* **2002**, *49*, 69.
18. Chang, J. H.; Park, D. K. *Polym. Bull.* **2003**, *51*, 69.
19. Solis-Sanchez, A.; Rejon-Garcia, A.; Manero, O. *Macromol. Symp.* **2003**, *192*, 281.
20. Imai, Y.; Inukai, Y.; Tateyama, H. *Polym. J.* **2003**, *35*, 230.
21. Chang, J. H.; Kim, S.-J.; Joo, Y.-L.; Im, S. S. *Polymer* **2004**, *45*, 919.
22. Folland, R. Proc. Pack Alimentaire, **1990**.
23. Cahill, P. J.; Chen, S. Y. B P Amoco Corporation, U.S. Patent, **2000**, 6,083,585.
24. Ching, T. Y.; Cai, G.; Depree, C.; Galland, M. S.; Goodrich, J. L.; Leonard, J. P.; Mathews, A.; Russell, K. W.; Yang, H. WO/1999/048963
25. Ching, T. Y.; Goodrich, J.; Cai, K.; Yang, H.; Oxygen Absorbers 2001 and Beyond Conference Proceedings, June, 2000, pages 36-42, in Chicago and organized by George O. Schroeder and Assiciates, **2000**.
26. Tharmapuram, S. R.; Jabarin, S. A. *Adv. Polym. Technol.* **2003**, *22*, 137.
27. Kim, S.-G.; Lofgren, E. A.; Jabarin, S. A. *J. Appl. Polym. Sci.*, **2012**, *127*, 2201.
28. Labde, R.; Lofgren, E. A.; Jabarin, S. A. *J. Appl. Polym. Sci.*, **2012**, *125*, issue S1, E369.
29. Reilly, J. F.; Limbach, A. P. *ANTEC'92*, **1992**, 112.
30. Lauritzen J. I.; Hoffman, J. D. *J. Appl. Phys.* **1973**, *44*, 4340.
31. Sadler D. M.; Gilmer, G. H. *Polymer* **1984**, *25*, 1446.
32. Powers, J.; Hoffman, J. D.; Weeks, J. J.; Quinn F. A. *J. Res. Natl Bur. Std.* **1965**, *69A* (4), 445.
33. Supaphol, P.; Spruiell, J.E.; Lin, J. S. *Polym. Int.* **2000**, *49*, 1473.
34. Zhou, C. X.; Clough, S. B. *Polym. Eng. Sci.* **1988**, *28*, 65.
35. Meares, P. In Polymers: Structure and Properties; D. Van Nostrand Company LTD.: Princeton, New Jersey, **1965**, 125–159.
36. Stein, R.S.; Powers, J. Topics in Polymer Physics, Chapter 8, The Crystalline State; Imperial College Press: London England, **2006**, 352–388.
37. Jabarin, S. A. *J. Appl. Polym. Sci.* **1987**, *34*, 85.
38. Patkar, M.; Jabarin, S. A. *J. Appl. Polym. Sci.* **1993**, *47*, 1749.
39. Wang, Z.-G.; Hsiao, B. S.; Sauer, B. B.; Kampert, W. G. *Polymer* **1999**, *40*, 4615.
40. Lim, G. B. A.; Lloyd, D. R. *Polym. Eng. Sci.* **1993**, *33*, 513.
41. Mahajan, K. Ph.D. Thesis, Polymer Institute, University of Toledo, **2010**.
42. Kenig, S.; Silberman, A.; Dolgopolsky, I. *ANTEC'97* **1997**, 2706.
43. Talukdar, M.; Achary, P. G. R. *Int. J. Res. Rev. Appl. Sci. (IJRRAS)* **2010**, *3*, 92.
44. Cobbs, W. H.; Burton, R. L. *J. Polym. Sci.* **1953**, *12*, 275.
45. Hartley, F. D.; Lord, F. W.; Morgan, L. B. *Phil Trans Roy Soc London* **1954**, *A247*, 23.